J. Phys. B: At. Mol. Opt. Phys. 26 (1993) 4845–4860. Printed in the UK

Differential electron scattering from acetylene—elastic scattering and vibrational excitation

M A Khakoo†, T Jayaweera‡, S Wang§ and S Trajmar§

† Department of Physics, Carliforia State University, Fullerton, CA 92634, USA
‡ Physics Department, Oberlin College, Oberlin, Ohio, USA
§ Jet Propulsion Laboratory, California Institute of Technology, Pasadena, CA 91109, USA

Received 22 June 1993

Abstract. Absolute differential cross sections for elastic scattering of electrons from acetylene are reported. The relative flow method was applied to normalize these cross sections, using helium as a standard. The measurements were made at the incident electron energies of 5 eV, 10 eV, 15 eV, 20 eV, 30 eV, 50 eV and 100 eV for electron scattering angles in the range of 10° to 125°. In addition, we report differential cross sections for excitation of the ν_1/ν_3 (unresolved), ν_2, ν_4/ν_5 (unresolved) and $\nu_4 + \nu_5$ vibrational modes of acetylene at 5 eV and 10 eV incident electron energies for scattering angles in the range of 20° to 120°. From these results integral cross sections are derived and the present results are compared with other available experimental and theoretical cross sections.

1. Introduction

Electron impact studies of simple, gaseous hydrocarbon molecules are of importance for several reasons. Hydrocarbons are present in planetary atmospheres and interstellar media where they play a significant role in the chemistry of these environments (Trajmar and Cartwright 1984). For example, acetylene (C_2H_2) is a trace constituent formed by the photodissociation of methane in the atmospheres of Jupiter, Saturn and Titan (Varanasi *et al* 1983, Broadfoot *et al* 1979) and its concentration in the Earth's atmosphere is also expected to nearly double by the year 2030 due to the increased use of automobiles (Varanasi *et al* 1983). Hydrocarbons are also used in the chemical vapour deposition (microchip) industry (Flamm 1989) where the carbon produced in the low-temperature discharges is used to harden substrates. Reactive species in these plasmas are produced by electron impact as a first step in the chain of chemical reactions. To develop viable models of the low-temperature hydrocarbon plasmas used one needs reliable electron scattering cross sections for such targets. Fusion plasma devices often use graphite as material for their inner walls in order to reduce radiation losses from such reactors. Hydrocarbon products are produced at these walls by reaction of the graphite with the deuterium fuel. The region close to these walls (plasma edge) plays an important role in the characteristics of the cold plasma edge as well as the hot plasma interior (Tawara and Phaneuf 1988, Tawara *et al* 1992). Developments in computational techniques have enabled the modelling of these complex targets with increased sophistication. Experimental data are also needed to test these models. A recent review of theoretical approaches to this problem is given by Gianturco and Jain (1986) who highlight the enhanced difficulty in the development of electron—polyatomic scattering models in comparison with electron—atom scattering models.

0953-4075/93/244845+16$07.50

An excellent review of available cross sections for electron scattering from gaseous hydrocarbon molecules is given by Tawara *et al* (1992). The review shows a paucity of such data which is especially severe for acetylene. It was for this reason that acetylene was selected for the present investigations.

The first angular electron scattering measurements from C_2H_2 were made by Hughes and McMillen (1933). They produced relative differential scattering cross sections (DCSs) for elastic scattering at electron impact energies (E_0) of 10 eV, 25 eV, 50 eV and 100 eV, with scattering angles (θ) ranging from 10° to 150°. However, their relative DCSs include contributions from excitation of the lowest vibrational levels. Later, elastic DCS measurements were made at E_0 values of 100 eV, 200 eV, 400 eV, 600 eV and 1000 eV and scattering angles of 3° to 130° by Fink *et al* (1975). Their DCSs were normalized to theory (independent atom model) at scattering angles greater than 40°. Kochem *et al* (1985) investigated the direct and resonant vibrational excitation DCS for E_0 values between 0.5 eV to 3.6 eV and θ from 5° to 110°. They only published the elastic DCS at $E_0 = 2$ eV for q in the range of 10° to 105° and, elastic DSC at $\theta = 90$ as a function of E_0. More recently, Andric and Hall (1988) investigated the resonant vibrational excitation of acetylene at E_0 from 1.5 eV to 8 eV, but reported only relative DCSs.

The first total electron—acetylene scattering cross sections (Q_{tot}) measurements were made by Bruche (1929) for E_0 in the range of 1 eV to 33 eV. Recently, Sueka and Mori (1988) measured Q_{tot} using a retarding potential, time-of-flight method for E_0 ranging from 1 eV to 400 eV.

Elastic scatterings DCSs have been calculated by Mu-Tao *et al* (1990) using a fixed-nuclei approximation and employing the Schwinger iterative method to handle the low angular momentum components of the scattered wave plus a Born closure treatment of the high angular momentum components. These intermediate energy calculations span the E_0 range of 10 eV to 200 eV.

In this paper, we present elastic scattering and vibration excitation DCSs for acetylene for E_0 from 5 eV to 100 eV and θ from 10° to 125°. In the present as well as in other earlier measurements, rotational excitation was not resolved from elastic scattering. At low impact energies significant contribution to the measured signal may also result from excitation of low-lying vibrational modes, ν_4 and ν_5. To correct the DCS at $E_0 = 5$ eV and 10 eV for these vibrational contaminations ($\approx 10\%$) we measured the DCS for excitation of the ν_1/ν_3, ν_2, ν_4/ν_5 and $\nu_4 + \nu_5$ vibrational modes (see Kochem *et al* 1985 for details of this notation). The DCSs were extrapolated and integrated to obtain corresponding integral cross sections. The present data are compared with other available DCS measurements and calculations.

2. Experiment

Since the experimental set-up has been described elsewhere (Khakoo and Trajmar 1986), only a brief description will be given here. A beam–beam geometry was used. The gas beam was aligned perpendicularly to the scattering plane defined by the electron gun and the detector axes. The electron spectrometer is composed of an electron gun and a scattered electron analyser, both using a hemispherical electrostatic energy selectors with virtual entrance and exit apertures and cylindrical electrostatic lenses. The electrons can be detected in the angular range of $\theta = -30°$ to 125° with an angular resolution of $\pm 1.5°$.

For elastic scattering measurements, the experiment was operated with an incident resolution of typically 70 meV to 90 meV (FWHM) at E_0 values of 5 eV to 100 eV,

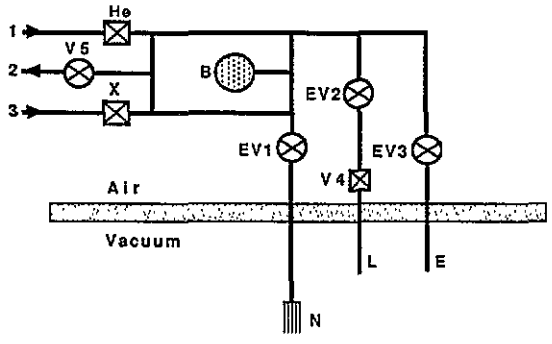

Figure 1. Schematic diagram of the gas handling system. B = Baratron, EV1, EV2 and EV3 are electric valves. V5 connects the system to a rotary pump used for quick evacuating or system flushing. N = capillary needle, L = background leak, E = exhaust to high vacuum. Arrows indicate direction of gas flow. See text for more discussion.

respectively. For vibrational excitation, the experiment was operated with 4 nA to 6 nA with an energy resolution of 40 meV to 50 meV. The experimental E_0 value was determined to a precision of ± 0.1 eV by observing the $1s2s^2$ well known Feshbach resonance feature in helium which takes place at $E_0 = 19.37$ eV. The magnetic field intensity in the vacuum chamber was checked using a fluxgate magnetometer and found to be approximately 1.5 mG around the collision region. The spectrometer was heated to approximately 100 °C using a thin biaxial inconel wire heater (total diameter 1 mm) to improve its stability from over a period of days to weeks. The vacuum chamber was pumped by an unbaffled 6″ Edwards Diffstack diffusion pump with Santovac-5 oil. To inhibit the backstreaming of rotary pump oil into our vacuum chamber, the rotary pump was charged with a low grade of diffusion pump oil (vapour pressure in the low 10^7 Torr). Further, a long backing line equipped with a 'micromaze' filter (K J Lesker Company, PA) was used. The background pressure in the chamber (no gas load) was about 4×10^{-8} Torr.

A diagram of the gas beam handling system is shown in figure 1. The tubing of this gas system was made of copper that was found to be relatively inert to C_2H_2, which is supposed to form copper acetylide on copper surfaces (Sueoka and Mori 1989, Outka *et al* 1983). This inertness was determined by filling all valves and observing any decrease of pressure with time. No change was found within the outgassing rate of this system (i.e. 0.1 mTorr min^{-1}). The gas was fed into the leak valves (see figure 1) through thick teflon tubing (1.5 mm wall thickness) from the gas cylinder using two-stage pressure regulators with stainless steel diaphragms. The system could be quickly evacuated down to > 0.1 Torr up to the gas cylinder heads, using an auxiliary rotary pump connected to valve V5. High purity helium (99.99%) and absorption grade C_2H_2 (99.7%) were used. This lower purity C_2H_2 is not expected to affect our measurements (see Sueoka and Mori 1989). Unfortunately, research grade C_2H_2 (99.999%) is very expensive. A temperature-stabilized baratron (figure 1) with a range of 1 mTorr to 10 Torr (accuracy $\pm 0.1\%$ of full scale) was used to monitor the gas pressure in the gas line.

To perform the absolute calibration of the C_2H_2 elastic DCS, the relative flow rates of the calibration gas (helium) and C_2H_2 must be known. To measure these relative flows rates, all the electrically operated valves were closed and the gas of interest was flowed into the piping through one of the leak valves—He (for helium) or X (for C_2H_2 or argon) in figure 1. The linear rise of the pressure with time in the baratron was recorded by computer, and its slope equals our relative flow rate (Khakoo and Trajmar 1986). Immediately following this, for the same setting of the leak valve, EV1 was opened, and the stabilized source drive pressure (SSDP) was determined. Since the viscosity of C_2H_2 is considerably larger than helium, this stabilization took considerably longer for C_2H_2 as compared with helium. The

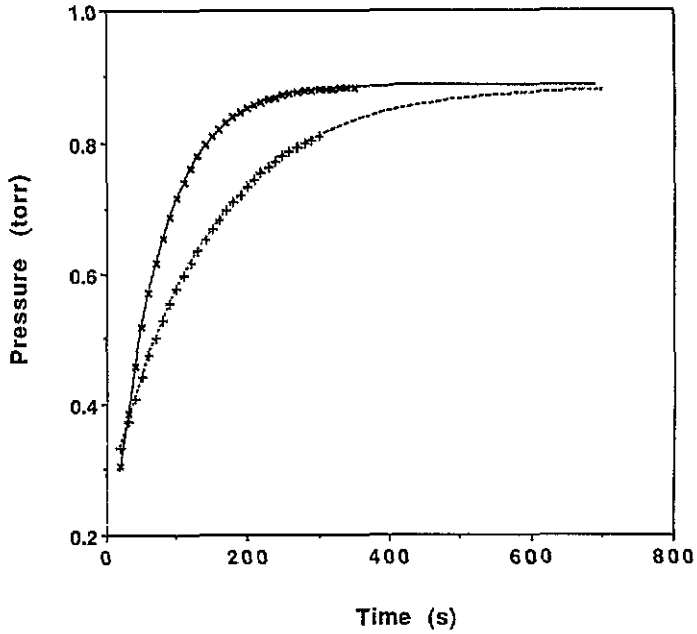

Figure 2. Typical pressure versus time data for helium and C_2H_2 showing the determination of the SSDP in the experiment. Legend: (×) helium data; (——) fit to equation (2) with ($P_\infty = 0.887 \pm 0.002$, $a = 0.0154 \pm 0.001$, $t_o = -6.3 \pm 0.3$); (+) C_2H_2 data; (- - - -) fit to equation (2) with ($P_\infty = 0.882 \pm 0.002$, $a = 0.0073 \pm 0.000\,06$; $t_0 = 45.5 \pm 0.$).

dependence of pressure (P) with time is of the form

$$\frac{dP}{dt} = \frac{1}{V}\frac{dn}{dt}kt - \alpha P \tag{1}$$

where V is the volume of the gas-handling piping, k is Boltzmann's constant, T is the temperature and α is the conductance for the exhaust part of the gas system leading to and including the gas needle. This equation assumes that the conductance is weakly dependent on P, and hence it is constant for a given setting of the leak valve (He or X). Equation (1) has the solution

$$P = P_\infty (1 - \exp -\alpha (t - t_0)) \tag{2}$$

where P_∞ equals the SSDP at this setting of the leak valve (i.e. the pressure at time $t = \infty$). t_0 is the experimental time offset from $t = 0$. We thus let the computer record the pressure-versus-time stabilization curve and fitted this curve to (2) using non-linear least-squares algorithms supplied by Press *et al* (1988). A sample of such data is shown in figure 2 together with the fit which in all cases was found to give values of P_∞ to within 2% error. This is a more efficient and reliable method if determining the SSDP, than manually waiting for the pressure to be close (within < 1%) to the SSDP. This method is also especially useful for gases with large viscosities (e.g. C_2H_2). We draw attention to the fact that the operating temperature of the experiment (110 °C) is above room temperature. Flow rates were thus also measured with the experiment at this temperature, and were reproducible within 3% in all cases.

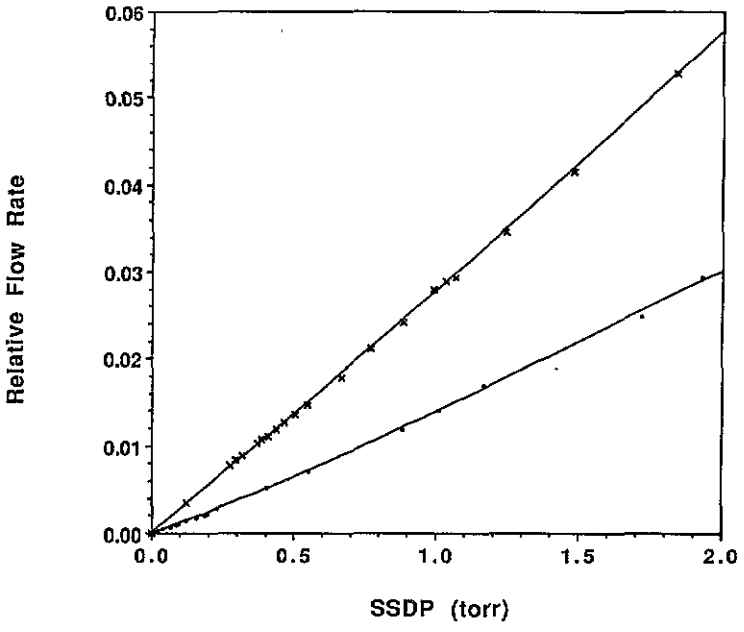

Figure 3. RFR versus SSDP for the present experimental set up. Legend: (×) helium and (•) C_2H_2; (——) polynomial fits to data points.

Using this system, we generated a series of data points of SSDP versus relative flow rate for helium, C_2H_2 and argon. The helium and C_2H_2 flow rates are plotted in figure 3 together with a polynomial fit which was used to determine the flow rate values for the SSDPs used during the experiment to a precision of less than 3% on average. In this way we were conveniently able to determine the relative flow rates, RFR, from the baratron reading of SSDP.

The method of relative flow requires that the unknown gas (X) and the calibrating gas (helium) be passed through the capillary array at their corresponding pressures P_X, P_{He} so that the mean free path for these gases is the same. Under these conditions the DCSs for elastic scattering for the two gases (i.e. DCS_{He}, DCS_X) are related by (see Nickel *et al* 1990)

$$\frac{DCS_X}{DCS_{He}} = \frac{RFR_{He}(P_{He})}{RFR_X(P_X)}\sqrt{\frac{M_{He}}{M_X}\frac{I_{eX}(E_0,\theta)}{I_{eHe}(E_0,\theta)}} \tag{3}$$

where RFR (P_X) represents the relative flow rates of the subscripted gases at the pressure P_X (e.g. for gas X), M their corresponding molecular weights and $I_{eX}(E_0,\theta)$, for example, is the scattered electron signal with gas X flowing at E_0 and θ.

The relative flow method additionally requires that the electron spectrometer perform with identical electron beam current and analyser detection characteristics for both gases. C_2H_2 caused considerable cooling of the electron filament, leading to a drift in the electron beam current. To reduce this drift the filament was operated at 20–30% greater power than normal. In addition the experiment was operated with the background C_2H_2 in the chamber $< 5 \times 10^{-7}$ Torr, so that this filament cooling effect was reduced and, on average, the electron beam did not vary by more than 5% during the entire run. This variation was taken into account by correcting the scattered electron signal for the accumulated Faraday cup current during the experiment.

The scattered electrons, for a fixed E_0 and θ, were energy analysed and then detected by a spiraltron detector. The pulses were handled by conventional pulse counting electronics. These pulses were fed into a PC computer which was operated in the multi-channel scaling mode. The computer also generated the linear energy loss ramp voltage and controlled the scattering angle (within $\pm 0.2°$) via a stepper motor and an angular potentiometer rigidly connected to the detector. The computer also controlled the gas beam electrical valve system shown in figure 1. A digital voltmeter coupled to a relay assembly was also linked to the computer (via an IEE488 bus). This enabled the computer to read various voltages used in controlling and monitoring the experiment, e.g. the baratron pressure in the target gas beam line, the energy loss, the incident electron energy, etc. The computer also monitored the incident electron current as measured by a deep Faraday cup placed downstream from the collision region, using an electrometer coupled to the same IEE488 bus. Consequently, the computer could store the average current and its standard deviation during a data run. The Faraday cup came in place when the detector angle exceeded 40°. Otherwise, it was pushed away by the detector. Thus, data taken for scattering angles less than 40° were sandwiched between data taken at larger angles to check the drifting of the electron beam, and the data were corrected linearly for this change. The computer would command the experiment to cover a complete range of angles in a pseudo-random order and scan the energy loss range of interest for a preset number of scans at each angle, and save the data, including the electron currents, beam pressures and spectrometer voltages, and proceed to the next scattering angle.

The procedure for acquiring elastic scattering data was as follows. With the spectrometer operating, the gas lines were purged with helium several times. Then helium was passed through the capillary at a known SSDP (≈ 0.75 Torr) and for the complete set of scattering angles the electron scattering signal was determined by scanning the elastic energy peak from -0.25 eV to 0.25 eV energy loss. The gas was then re-routed through the preset leak, 'L' in figure 1 (adjusted to be similar in conductance to the capillary) and the background contribution to the scattered electron signal was determined. Then, the helium was pumped out through V5 (figure 1) and the gas lines were purged with C_2H_2. The experiment was repeated with C_2H_2 at the SSDP (≈ 0.15 Torr) where its estimated mean free path was close to that of helium, i.e.

$$\frac{P_{He}}{P_{C_2H_2}} = \frac{\sigma^2_{C_2H_2}}{\sigma^2_{He}} \tag{4}$$

where σ_{He} ($= 2.20 \times 10^{-10}$ m) and $\sigma_{C_2H_2}$ ($= 4.96 \times 10^{-10}$ m) are the molecular diameters for these gases (Roth 1978). Finally, the C_2H_2 was replaced by helium and the experiment was repeated to check on possible instabilities or drifts. This procedure was also carried out for argon at $E_0 = 20$ eV, again using helium as a DCS standard. From the above data we determined absolute DCS values of C_2H_2 and argon using (3). The helium DCSs were taken from Register *et al* (1980), or where these data were unavailable, from the variational calculations of Nesbet (1979).

The absolute value of the elastic C_2H_2 elastic DCSs could be reproduced to better than 12% and gave good agreement (within 7% to 12%) with available argon DCS (Srivastava *et al* 1981 and Furst *et al* 1989). Further, we found that the reproducibility of the angular distribution of the C_2H_2 elastic DCS is $< 8\%$. Several factors may be responsible for this. The accuracy of the relative flow method in our experiment may be influenced by how precisely we could reproduce the conditions required by (4). Additionally, the electron optics of our spectrometer may be varying due to absorption of gas onto the spectrometer

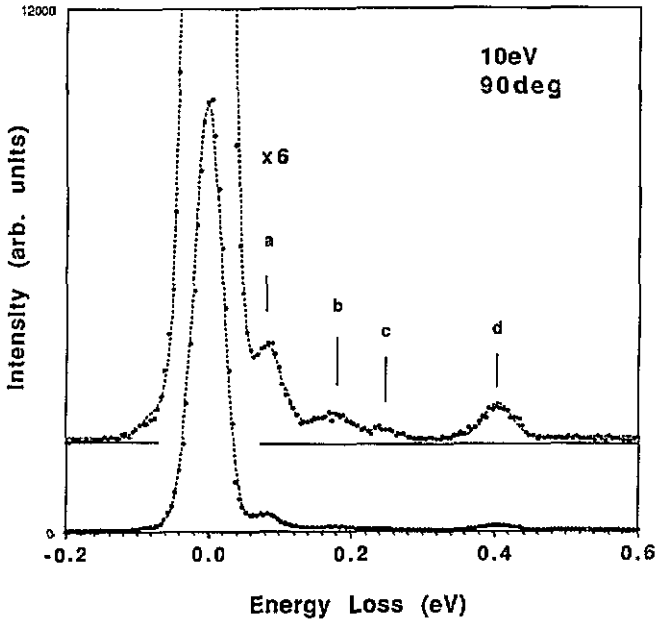

Figure 4. A typical spectrum of C_2H_2 taken with 50 meV FWHM resolution at $E_0 = 10$ eV and $\theta = 90°$. The dotted curve is a synthetic fit to the spectrum (see text). Features labelled a–d are vibrational excitations of ν_4/ν_5, $\nu_4 + \nu_5$, ν_2 and ν_1/ν_3 modes, respectively.

lenses. We also repeated the measurements at several angles, changing from helium to C_2H_2 and back. Approximately the same amount of variation (about 14%) in the absolute normalization was found.

Since we encountered this difficulty with the C_2H_2 measurements and since we disagreed with available experimental DCS data at 100 eV and theoretical results in general, we decided to carry a further check on our absolute DCS calibration. A static gas DCS calibration was carried out. We calibrated our ionization gauge against an absolute baratron at pressures in the range of 5×10^{-6} to 8×10^{-5} Torr for both helium and acetylene. This calibration of the ionization gauge was linearly extrapolated to pressures below 5×10^{-6}. Electron scattering measurements with the static gas were then performed for helium and C_2H_2 for θ of 60° and 90°, using the calibrated ionization gauge to determine the pressure of our static gas target which filled the vacuum chamber. In this experiment, the ionization gauge was frequently degassed to avoid contamination. The DCSs from this static gas arrangement are given by

$$\frac{\mathrm{DCS_X}}{\mathrm{DCS_{He}}} = \frac{P^i_{\mathrm{He}}}{P^i_{\mathrm{X}}} \frac{I_{\mathrm{eX}}(E_0, \theta)}{I_{\mathrm{eHe}}(E_0, \theta)} \tag{5}$$

where P^i_{He}, P^i_{X} are the (calibrated) ionization gauge pressures for helium and C_2H_2. The background contribution to the electron scattering signal in the static gas setup was determined by shutting off the gas. Since the signal rates for the static gas measurements were considerably lower than those for the gas beam, the static gas cell experiment was performed at $E_0 < 30$ eV, i.e. where the magnitude of these DCSs are large enough to provide satisfactory statistics (< 3%). Agreement with our relative flow C_2H_2 DCS was excellent, i.e. in all cases within experimental errors.

Table 1. Differential and integral elastic scattering cross sections. Units: (DCS)$\times 10^{-16}$ cm^2 sr^{-1}, (integral) $\times 10^{-16}$ cm^2.

	Impact energy						
Angle (deg)	5 eV	10 eV	15 eV	20 eV	30 eV	50 eV	100 eV
10				8.97	6.58	8.38	4.94
15	5.05	8.77	7.11	6.45	5.71	6.40	2.53
20	4.20	6.62	5.53	5.38	4.55	3.78	1.14
25	3.62	5.36	4.02	4.11	3.34	2.00	0.74
30	3.02	3.92	2.94	3.02	2.15	1.29	0.48
35	2.55	3.28	2.16	2.10	1.33	0.76	0.32
40	2.18	2.43	1.69	1.55	1.04	0.54	0.24
45	1.96	1.89	1.42	1.20	0.77	0.41	0.18
50	1.77	1.62	1.19	0.94	0.64	0.29	0.13
60	1.35	1.31	0.87	0.64	0.44	0.15	0.10
70	1.23	1.06	0.72	0.47	0.30	0.12	0.07
80	1.00	0.91	0.63	0.46	0.24	0.10	0.06
90	0.98	0.90	0.65	0.47	0.23	0.10	0.06
100	1.11	0.98	0.65	0.46	0.19	0.10	0.05
110	1.17	1.02	0.67	0.43	0.19	0.11	0.05
120	1.33	1.06	0.72	0.46	0.22	0.12	0.05
125	1.40	1.13	0.73	0.49	0.27	0.13	0.06
Average error (%)	14.5	13.6	13.5	13.6	14.6	14.3	15.1
Integral	20.3	20.3	15.1	12.8	8.5	5.6	3.7
Error (%)	17.8	18.2	18.5	18.7	19.0	10.1	21.0

In the present measurements, rotational excitation was not distinguished from elastic scattering. The measured elastic scattering DCS therefore represent elastic scattering plus rotational excitation. In addition, the elastic energy loss feature of C_2H_2 of the relative flow data was contaminated by the ν_4/ν_5 vibrational excitation energy loss feature. This contamination was observed to be significant at low energies. To correct our elastic scattering DCSs for vibrational excitation at low E_0 values, we took electron energy loss spectra at $E_0 = 5$ eV and 10 eV in the θ range of 20° to 120°, using a higher energy resolution as mentioned earlier. A representative energy loss spectrum is shown in figure 4. To obtain good scattered electron rates, pressure in the chamber was typically 3×10^{-6} for a SSDP of 0.5 Torr. These spectra were fitted using a multi-Gaussian instrumental line function determined from the elastic peak. This unfolding determined the intensity ratios of vibrational excitation features to the elastic peak. By normalizing these ratios to the elastic DCSs for C_2H_2 we determined the vibrational excitation DCSs as well as decontaminating our elastic DCS data from vibrational excitation. We estimate that for $E_0 > 10$ eV the vibrational contribution to the elastic DCS is $< 5\%$ and therefore have not attempted to make any further corrections of the C_2H_2 elastic DCSs for $E_0 > 10$ eV.

3. Results and discussion

The differential and integral elastic cross sections with their (average) errors are given in table 1. Differential vibrational excitation DSCs are given in table 2. The DCSs are plotted along with other available DCSs in figures 5 to 10. The integral elastic cross sections are shown in figure 11. Finally, vibrational excitation DCSs are plotted in figures 12 and 13.

Table 2. Differential and integral vibrational excitation cross sections for $E_0 = 5$ eV and 10 eV. See table 3 for sources of errors. Units: (DCS) $\times 10^{-18}$ cm^2 sr^{-1}, (integral) $\times 10^{-18}$ cm^2.

	5 eV				10 eV			
Angle (deg)	ν_4/ν_5	$\nu_4+\nu_5$	ν_2	ν_1/ν_3	ν_4/ν_5	$\nu_4+\nu_5$	ν_2	ν_3/ν_1
20	34	14		4.5	16	8.1		2.2
30	17	6.9	0.66	2.7	7.3	4.2		1.2
40	12	4.6	0.55	2.3	4.5	2.7		0.91
50	11	3.9	0.68	2.5	4.5	2.1	0.27	0.93
60	9.1	3.1	0.75	2.2	5.0	1.8	0.29	1.3
70	8.8	2.8	0.73	2.6	4.6	1.6	0.27	1.5
80	8.0	2.5	0.95	3.0	5.5	1.3	0.25	1.4
90	7.5	2.2	1.1	3.6	5.9	1.4	0.27	1.3
100	7.4	2.4	1.4	2.7	6.0	1.6	0.37	1.4
110	8.4	2.2	1.3	3.1	5.7	1.5	0.47	1.6
120	6.6	2.5	1.5	2.7	3.9	1.3	0.87	2.1
Integral	122	44	14	34	69	26	5.9	18
Error (%)	35	36	38	36	37	38	41	39

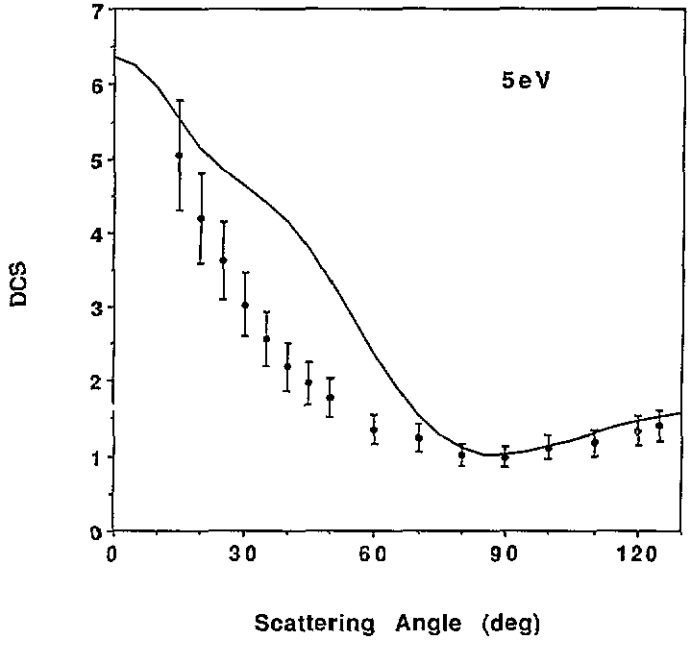

Figure 5. C_2H_2 elastic scattering DCS values at $E_0 = 5$ eV. Legend: (•) present work; (——) Jain (1992). Units: $\times 10^{-16}$ cm^2 sr^{-1}.

A summary of contributing errors is given in table 3. The relative elastic DCS error is the sum of errors due to the electron and gas beam instabilities, statistical (Poisson) errors of the scattered electron signal and the errors quoted on the helium DCSs used for calibration, all added together in quadrature. The error on the absolute DCS is the sum of the relative elastic DCS error and the absolute DCS normalization error added in quadrature. The error in the vibrational DCSs is obtained from the sum of the elastic DCS error, statistical (Poisson) and spectrum unfolding (fitting) errors added in quadrature.

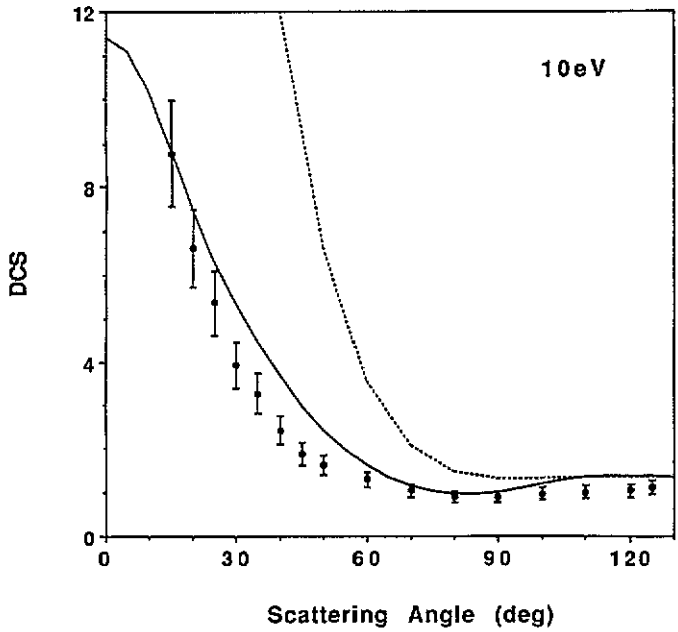

Figure 6. C_2H_2 elastic scattering DCS values at $E_0 = 10$ eV. Same legend as figure 5 except (----) Mu-Tao *et al* (1990). Units: $\times 10^{-16}$ cm^2 sr^{-1}.

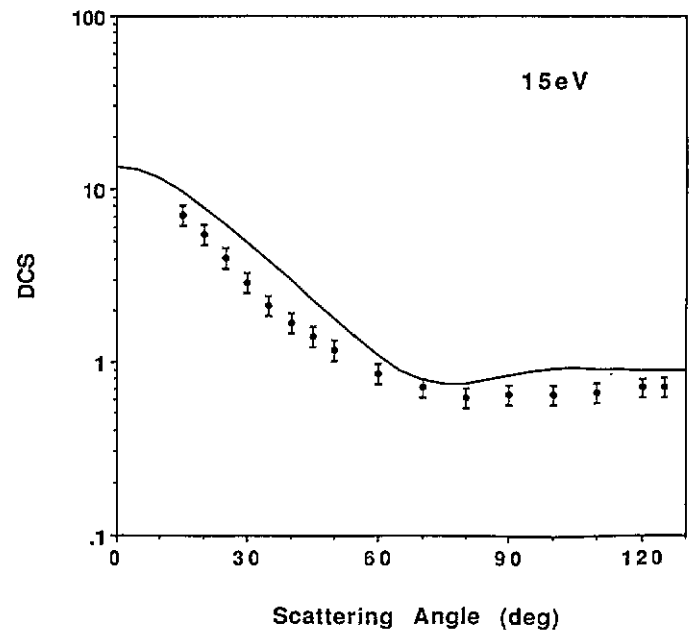

Figure 7. C_2H_2 elastic scattering DCS values at $E_0 = 15$ eV. Same legend as figure 5. Units: $\times 10^{-16}$ cm^2 sr^{-1}.

3.1. Elastic scattering

As seen in figure 5, at $E_0 = 5$ eV the present DCSs are in good agreement with the close-coupling (CC) calculations of Jain (1992) at $\theta > 90°$. However, significant differences occur

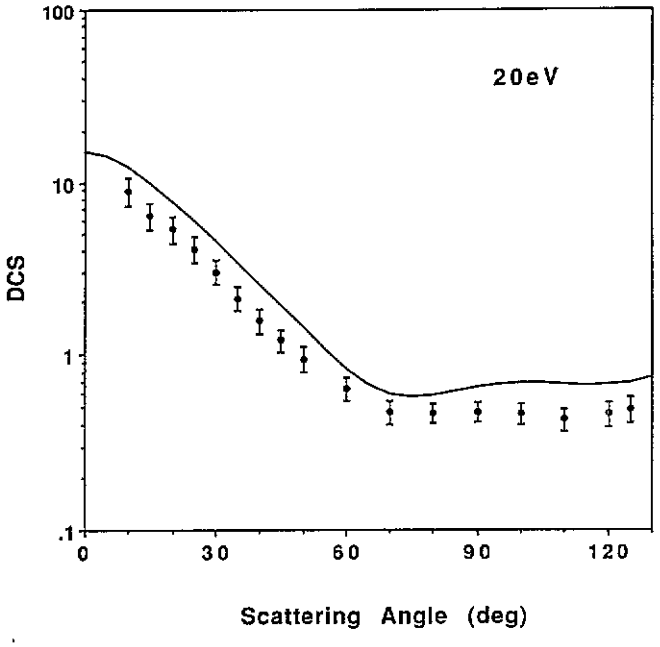

Figure 8. C_2H_2 elastic scattering DCS values at $E_0 = 20$ eV. Same legend as figure 5. Units: $\times 10^{-16}$ cm^2 sr^{-1}.

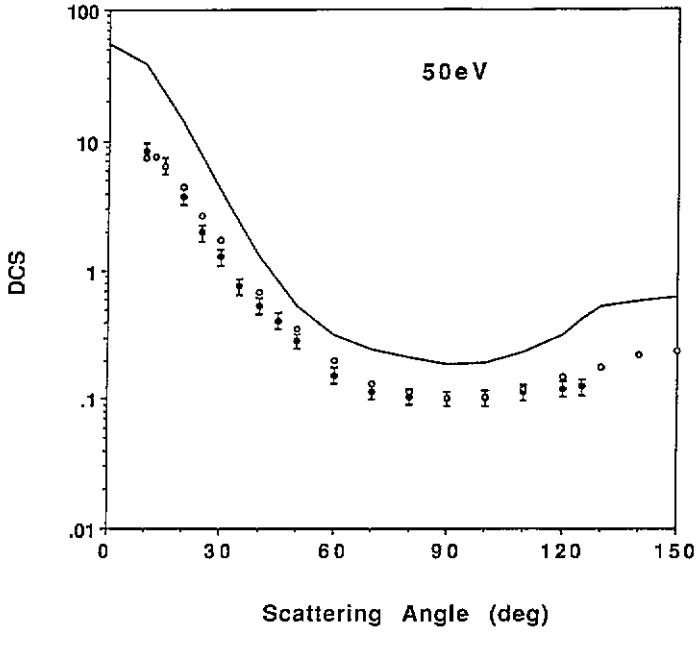

Figure 9. C_2H_2 elastic scattering DCS values at $E_0 = 50$ eV. Legend: (•) present work; (——) Mu-Tao (1990); (○) Hughes and McMillen (1993) normalized to present work at $\theta = 90°$. Units: $\times 10^{-16}$ cm^2 sr^{-1}.

at small scattering angles where our measurements do not reproduce the steep rise in his

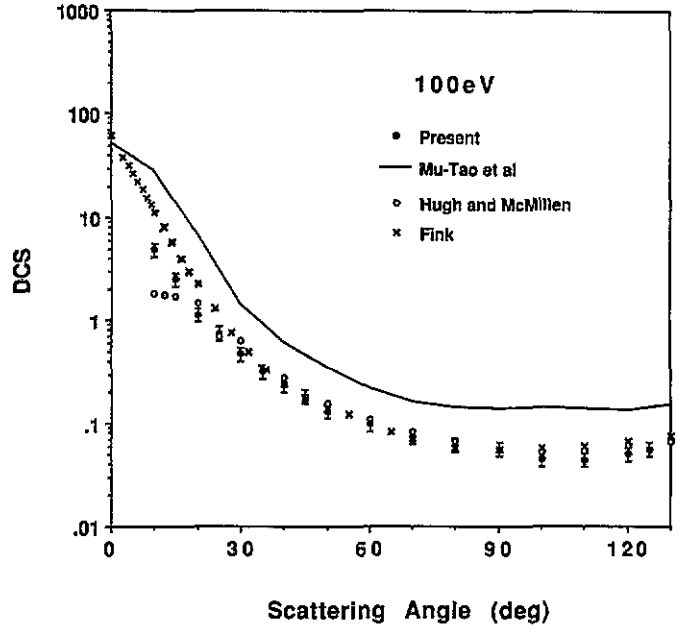

Figure 10. C_2H_2 elastic scattering DCS values at $E_0 = 100$ eV. Legend: (•) present work; (——) Mu-Tao (1990); (○) Hughes and McMillen (1993) normalized to present work at $\theta = 90°$; (×) Fink *et al* (1975) normalized to present work at $\theta = 90°$ (see text). Units: $\times 10^{-16}$ cm^2 sr^{-1}.

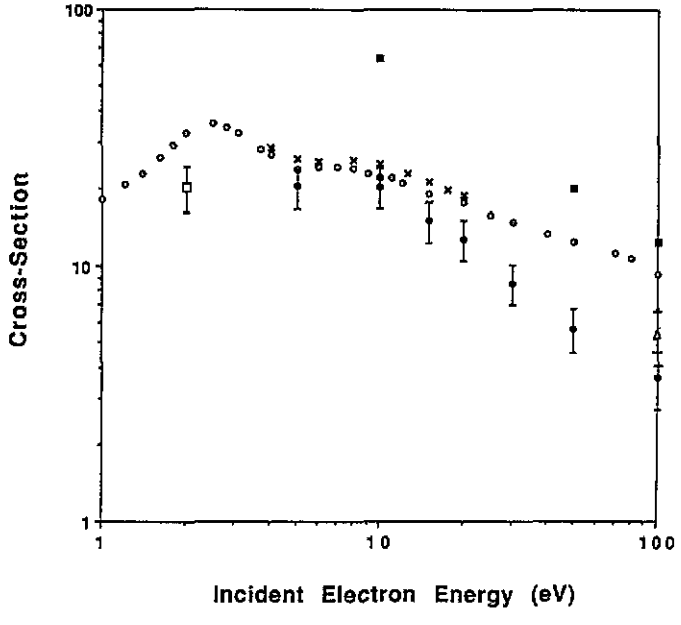

Figure 11. C_2H_2 total (Q_{tot}) and integral elastic (Q_{elas}) cross section values. Legend: (•) present work (Q_{elas}); (□) Kochem *et al* (1985) (Q_{elas}); (△) Fink *et al* (1975) (Q_{elas}), normalized to present work, see text; (×) Jain (1992) (Q_{elas}); (△) Mu-Tao *et al* (1990) (Q_{elas}); (○) Sueoka and Mori (1989) (Q_{tot}). Units: $\times 10^{-16}$ cm^2.

DCS values around $\theta > 40°$. The agreement at $E_0 = 10$ eV (figure 6) is very good, since

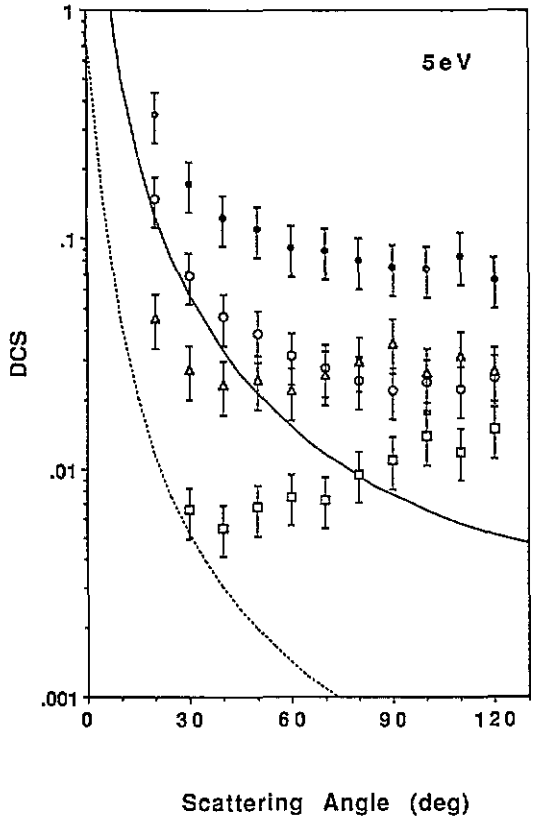

Figure 12. Present C_2H_2 vibrational excitation DCS at $E_0 = 5$ eV. Legend: (•) ν_4/ν_5; (○) $\nu_4 + \nu_5$; (□) ν_2; (△) ν_1/ν_3 vibrational modes. (——) ν_5 Born-dipole curve; (- - - -) ν_3 Born-dipole curve (see text). Units: $\times 10^{-18}$ cm^2 sr^{-1}.

Table 3. Summary of sources of errors. Errors are given in percentages. See text for further discussion.

Elastic							
Impact energy(eV)	Electron beam	Gas beam	Average statistical	Helium DCS	Relative DCS	Relative Flow normalisation	Total
5	3.0	4.0	2.3	5.0	7.4	12.5	14.5
10	2.0	4.0	2.7	5.0	7.2	11.5	13.6
15	3.0	4.0	2.5	5.0	7.5	11.2	13.5
20	2.0	4.0	2.4	5.0	7.1	11.6	13.6
30	1.0	4.0	3.0	7.0	8.7	11.7	14.6
50	1.0	4.0	3.5	6.0	8.1	11.8	14.3
100	1.0	4.0	3.5	7.5	9.2	12.0	15.1

Vibrational excitation				
Impact energy (eV)	Elastic DCS	Statistical	Fitting	Total
5	14.5	5.2	19.2	24.6
10	13.6	6.0	21.8	26.4

both the experiment and the CC data are on average less than 20% apart. A broad minimum in the elastic scattering DCSs at approximately $\theta = 85°$ is clearly displayed by both sets of

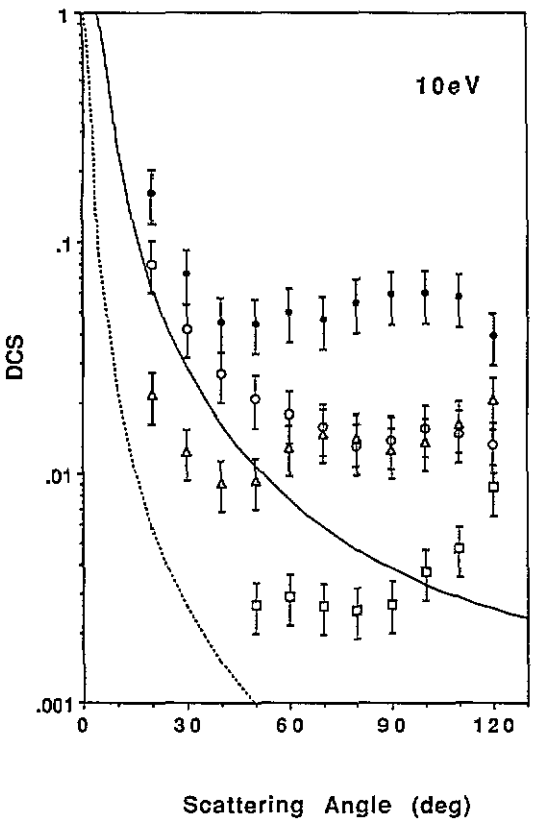

Figure 13. Present C_2H_2 vibrational excitation DCS at $E_0 = 10$ eV. Legend: (•) ν_4/ν_5; (○) $\nu_4 + \nu_5$; (□) ν_2; (△) ν_1/ν_3 vibrational modes. (——) ν_5 Born-dipole curve; (- - - -) ν_3 Born-dipole curve (see text). Units: $\times 10^{-18}$ cm^2 sr^{-1}.

data. On the other hand, the data of Mu-Tao *et al* (1990) at this E_0 are found to be too high by about as much as a factor of 5 in places. This is, however, not unexpected, since their method is physically not applicable at low energies. At $E_0 = 15$ eV (see figure 7) our DCSs are lower (by about 40% in places) than the CC values. Qualitatively, the experimental and theoretical DCSs are in very good agreement. At 20 eV (figure 8), qualitative agreement between the CC results and our DCSs is excellent to the extent of reproducing the structure from $\theta = 60°$ to $\theta = 125°$, but our DCSs are lower than the CC DCS values (by about 50%) i.e. representing a worsening of the situation with respect to $E_0 = 30$ eV.

At $E_0 = 50$ eV (figure 9), the agreement between our DCSs, the relative DCSs of Hughes and McMillen (1933) and the calculated DCSs of Mu-Tao *et al* (1990) is qualitatively excellent. Quantitatively, our DCSs and theory are in serious disagreement (by a factor of approximately 2). At $E_0 = 100$ eV (see figure 10), we find our measurements in disagreement with the absolute DCS values of Fink *et al* (1975) (which were normalized to the independent atom model) and Mu-Tao *et al* (1990) by approximately a factor of 3. Nevertheless, all the data sets remain in very good qualitative agreement. We have thus renormalized the DCSs of Fink *et al* to our DCS at $\theta = 90°$, for better comparison.

In figure 11, we show Q_{tot} and integral elastic cross sections (Q_{elas}) as a function of impact energy. The Q_{tot} values of Sueoka and Mori (1989) are given with an accuracy of about 8% in this range of impact energies. Below 5 eV impact energy the difference between Q_{tot} and Q_{elas} represents the sum of integral vibrational excitation cross sections. Above $E_0 = 4.5$ eV and 11.4 eV, electronic state excitations (Q_{elec}) and ionization (Q_{ion}) cross

sections, respectively contribute to Q_{tot} beside vibrational excitation. Comparison of our Q_{elas} with the Q_{tot} of Sueoka and Mori at $E_0 = 5$ eV and 10 eV gives reasonable agreement, i.e. when we add the integral cross section for vibrational excitation (about 20–30%, see next section) to our Q_{elas} we fall into reasonable agreement with the Q_{tot} within error limits. At $E_0 = 100$ eV if we add the total ionization cross section measurement of Gaudin and Hagemann (1967) ($Q_{ion} = 4.17 \times 10^{-16}$ cm H_2) to our value of $Q_{elas} = 3.66 \times 10^{-16}$ cm^2, we get the value of 7.83×10^{-16} cm^2 which is about 22% lower than the Q_{tot}, meaning that the remaining cross section (total inelastic, $Q_{inel} = Q_{tot} - Q_{elas} - Q_{ion}$), must be approximately 1.46×10^{-16} cm^2, and approximately half of the elastic cross section. This seems a reasonable situation, but one that needs to be confirmed independently. The Q_{elas} of Fink *et al* (1975) exceeds the Q_{tot} data, indicating that their absolute normalization to the independent-atom model may be an overestimate of the elastic scattering cross section. However, when we renormalize their DCSs, the situation is much improved.

3.2. Vibrational excitation

Figures 12 and 13 show the vibrational excitation DCS values at $E_0 = 5$ eV and 10 eV. Typical errors and their sources are given in table 3. Similarly to Kochem *et al* (1985), we could not resolve the ν_4/ν_5 and ν_1/ν_3 composite features with our present energy resolution (typically 50 meV). At 5 eV the DCS for excitation of the ν_4/ν_5 feature shows a forward-peaking characteristic of a dipole-type transition, i.e. the dominance of the infra-red active ν_5 vibrational mode, since the ν_4 component is Raman-active, hence non-dipole. Also shown is the Born-dipole curve at this energy. The DCS form of the Born-dipole approximation is related to the dipole transition moment (D) by

$$\mathrm{DCS} = \frac{4\kappa D^2}{3k^2} \frac{1}{(1 + \kappa^2 - \kappa\cos\theta)} \tag{6}$$

where κ is the ratio between the final and incident wave vector and k^2 is the incident energy in Rydbergs. The Born-dipole curve using D from Bishop and Cheung (1982), is in disagreement with our results. This is not surprising at this energy, since the effect of non-dipole interactions due to the ν_4 vibrational mode becomes significant at non-zero θ. The next feature which is the joint excitation of the $\nu_4 + \nu_5$ vibrational modes also shows forward peaking but is weaker than the ν_4/ν_5 feature. The ν_2 feature at 245 meV energy loss is backward peaked, consistent with the excitation of a Raman type of transition (Kochem *et al* 1985). The ν_1/ν_3 feature at approximately 400 meV energy loss shows a significantly lower forward peaking (possibly due to the lower dipole moment of the ν_3 mode as compared with the ν_5 mode (see Bishop and Cheung 1982) and a hump centred about $\theta = 90°$.

At 10 eV impact energy, the deviation of the forward-peaked DCS for excitation of the $\nu_4 + \nu_5$ feature DCSs still shows backward peaking as it did at $E_0 = 5$ eV, whilst the ν_1/ν_3 feature displays a complicated angular behaviour, i.e. a forward peaking DCS (due to the ν_3 component) with an increase at backward scattering angles and a small hump around $\theta = 70°$ probably due to the ν_1 component.

4. Conclusions

The present DCS measurements for elastic electron scattering from C_2H_2 show that the magnitude of the cross sections stays consistent with the Q_{tot} measurements of Sueoka and Mori (1989). At $E_0 = 100$ eV, when our elastic DCSs are integrated and added to the

available ionization cross section of Gaudin and Hagemann (1967) they give a reasonable agreement with the Q_{tot} of Sueoka and Mori, but indicate that the elastic DCSs of Fink *et al* (1975) are too high. The present elastic scattering DCSs show very good qualitative agreement with the available theoretical and other experimental DCSs. Still, large quantitative discrepancies exist between the present elastic DCSs and other available elastic DCSs.

Acknowledgments

This work was supported by a grant from the American Chemical SocietyPetroleum Research Fund no 23704-B6 and by the National Aeronautics and Space Agency. We acknowledge discussions with Dr A Jain and for his data prior to publication. We also acknowledge the technical help of Mr H Fabris, Mr J Buell and Mr T Timpe.

References

Andric L and Hall R I 1988 *J. Phys. B: At. Mol. Opt. Phys.* **21** 355
Bishop D M and Cheung L M 1982 *J. Phys. Chem. Ref. Data* **11** 119
Broadfoot A L *et al* 1979 *Nature* **204** 979
Bruche E 1929 *Ann. Phys., Lpz* **2** 909
Fink M, Jost K and Hermann D 1975 *J. Chem. Phys.* **63** 1985
Flamm D L 1989 Introduction to Plasma Chemistry *Plasma Etching—an Introduction* ed D M Manos and D L Flamm (New York: Academic)
Furst J E, Golden D E, Mahgerefteh M, Zhou J and Mueller D 1989 *Phys. Rev.* A **40** 5592
Gaudin A and Hagemann R 1967 *J. Chim. Phys.* **64** 1209
Gianturco F A and Jain A 1986 *Phys. Rep.* **143** 347
Hughes L and McMillen J H 1933 *Phys. Rev.* **44** 876
Jain A 1992 private communication
Khakoo M A and Trajmar S 1986 *Phys. Rev.* A **34** 138.
Kochem K-H, Sohn W, Jung K, Ehrhardt H and Chang E S 1985 *J. Phys. B: At. Mol. Phys.* **18** 1253
Mu-Tao L, Brescansin L, Lima M A P, Machado L E and Leal E P 1990 *J. Phys. B: At. Mol. Opt. Phys.* **23** 4331
Nesbet R K 1979 *Phys. Rev.* A **20** 58
Nickel J, Zetner P W, Shen G and Trajmar S 1991 *J. Phys. E: Sci. Instrum.* **22** 1325
Outka D A, Friend C M, Jorgensen S and Madix R J 1983 *J. Am. Chem. Soc.* **105** 3468
Press W H, Flannery B P, Teukolsky S A and Vetterling W T 1988 *Numerical Recipes* (Cambridge: Cambridge University Press)
Register D F, Trajmar S and Srivastava S K 1980 *Phys. Rev.* A **21** 1134
Roth A 1987 *Vacuum Technology* (New York: Elsevier)
Srivastava S K, Chutjian A and Trajmar S 1975 *J. Chem. Phys.* **63** 2659
Srivastava S K, Tanaka H, Chutjian A and Trajmar S 1981 *Phys. Rev.* A **23** 2156
Sueoka O and Mori S 1989 *J. Phys. B: At. Mol. Opt. Phys.* **22** 963
Tawara H and Phaneuf R A 1988 *Comment. At. Mol. Phys.* **21** 177
Tawara H, Itikawa Y, Nishimura H, Tanaka H and Nakamura Y 1992 *Nucl. Fusion Suppl.* **2** 41
Trajmar S and Cartwright D C 1984 *Electron–molecule Interactions and their Applications* (New York: Academic) vol 1 p 155
Varanasi P, Giver L P and Valero F P J 1983 *J. Quant. Spectrosc. Radiat. Transfer.* **30** 497